Corrigendum to The Cryosphere, 15, 2041–2055, 2021
https://doi.org/10.5194/tc-15-2041-2021-corrigendum

The Cryosphere
Open Access

Corrigendum to "Top-of-permafrost ground ice indicated by remotely sensed late-season subsidence" published in The Cryosphere, 15, 2041–2055, 2021

Simon Zwieback and Franz J. Meyer

Geophysical Institute, University of Alaska Fairbanks, Fairbanks, AK, USA

Correspondence: Simon Zwieback (szwieback@alaska.edu)

Published: 19 October 2023

The original article contains erroneous displacement estimates derived from Sentinel-1 InSAR (Interferometric Synthetic Aperture Radar). All values were too large by a factor of 2 so that a typical late-season subsidence observation over ice-rich terrain was 3 cm instead of the 6 cm originally reported.

The error was introduced by a coding error when computing the displacement d from the phase $\phi = 2kd$. In the evaluation of the wavenumber $k = 2\pi/\lambda$ from the wavelength λ, the factor of 2 was inadvertently omitted.

The error does not affect the separability of ice-poor and ice-rich terrain from InSAR, as quantified by the overlap of the late-season subsidence distributions. However, it needs to be considered for interpretation, model evaluation, and spatiotemporal comparisons. A late-season subsidence of ~ 3 instead of ~ 6 cm corresponds to substantially less excess ground ice melt in the extreme summer of 2019 than originally inferred. Also, lower late-season subsidence estimates of ~ 3 cm over ice-rich terrain remain larger than systematic errors of dielectric origin of ~ 1 cm.

We apologize for the error and thank Chen Jie for drawing our attention to it.

All relevant figures have been recompiled to facilitate interpretation of the results. They are reproduced below, and Figs. S2 and S3 have been updated in the Supplement. The data repository (https://doi.org/10.5281/zenodo.8408834, Zwieback, 2023) has also been updated.

References

Copernicus Sentinel: Copernicus Open Access Hub, available at: https://scihub.copernicus.eu, last access: 3 October 2020.

Planet Team: Planet Application Program Interface: In Space for Life on Earth, San Francisco, CA, https://api.planet.com, last access: 20 September 2020.

Zwieback, S.: Kivalina subsidence observations (1.1), Zenodo [data set], https://doi.org/10.5281/zenodo.8408834, 2023.

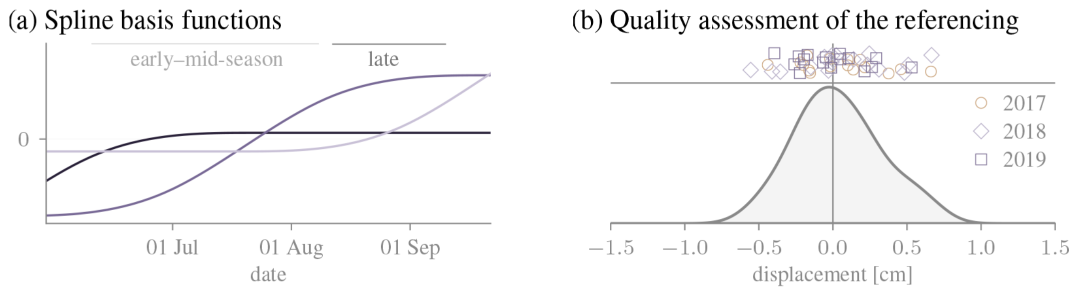

Figure 3. Late-season and early–mid-season subsidence were reconstructed by spline fitting and their accuracy assessed at stable validation points. **(a)** Three cubic spline basis functions, corresponding to decelerating, S-shaped, and accelerating subseasonal subsidence; for display purposes, we normalized them so that the peak subsidence rate is $1\,\mathrm{mm\,d^{-1}}$. **(b)** Reconstructed displacements over the validation points during the early-to-mid-season and late season (d_e and d_l, respectively; positive values corresponding to subsidence). Individual values for all points and years are shown at the top and a kernel density estimate of the distribution below.

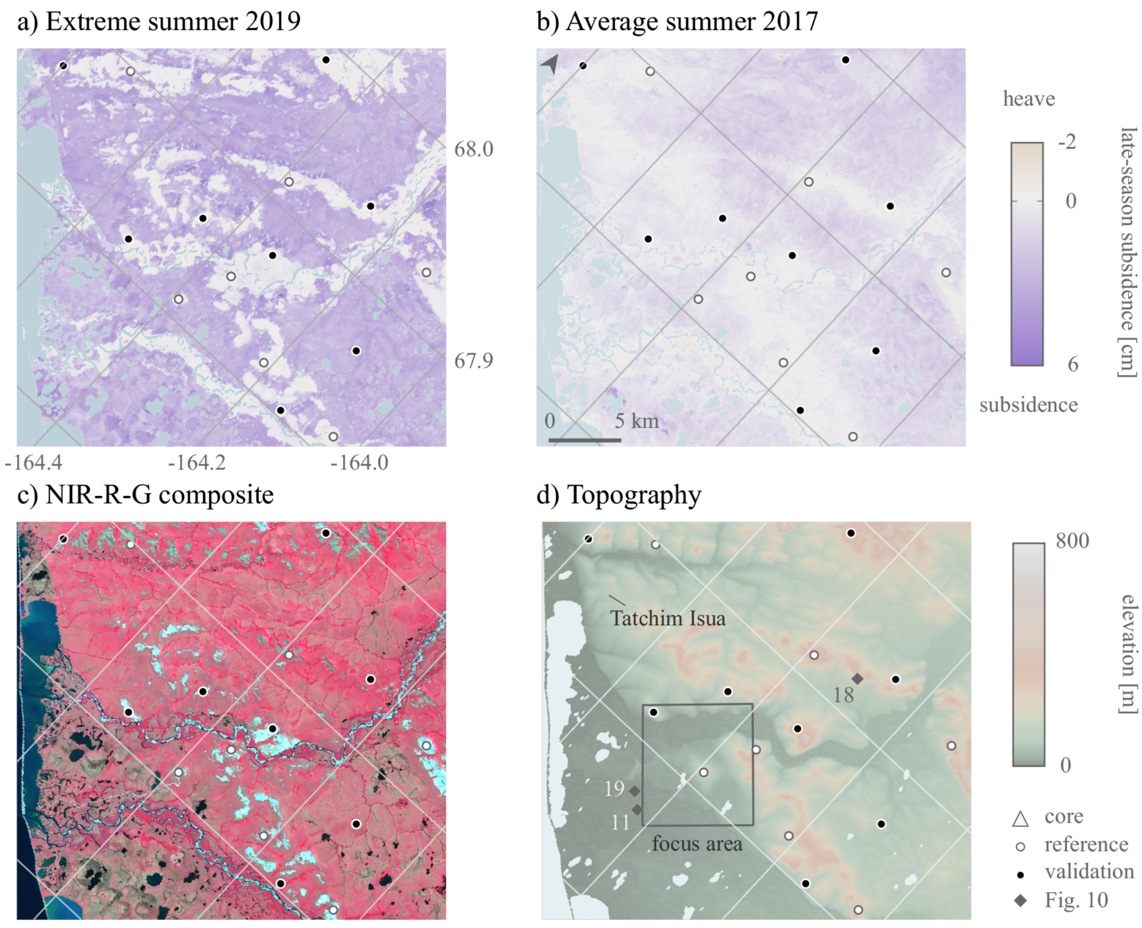

Figure 5. Remotely sensed late-season subsidence d_l within the study area, defined in Fig. 2; **(a)** d_l in the exceptionally warm summer of 2019; **(b)** d_l in the average summer of 2017. Positive values correspond to subsidence between 10 August and 10 September and negative values to heave during the same period. Missing values are shown in light blue. **(c)** Sentinel-2 false-colour composite image (Copernicus Sentinel, 2020); **(d)** topography estimated from the TanDEM-X DEM. The reference and validation points (Sect. 3.1.3) for the Sentinel-1 subsidence estimates are indicated by white and black circles, respectively; the locations of the ground ice cores are shown by triangles; the labelled diamonds refer to points shown in Fig. 10. The focus area for manual mapping and the Tatchim Isua candidate relocation site are shown in **(d)**.

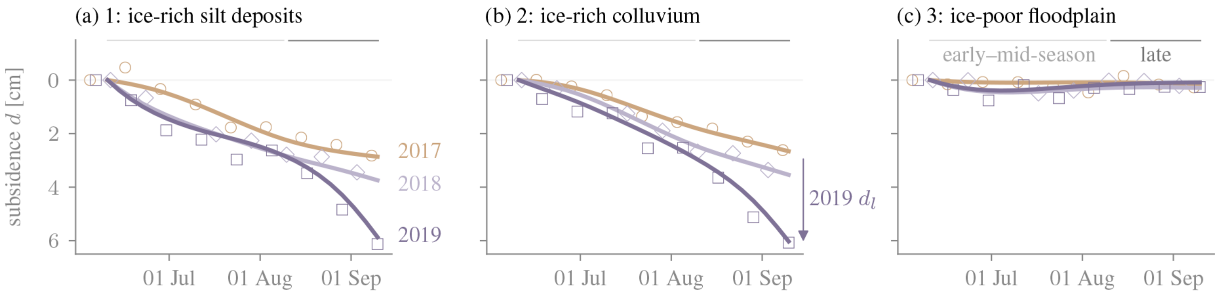

Figure 6. Cumulative subseasonal subsidence (line: spline fit, markers: unconstrained) from all 3 years. The late-season subsidence (10 August–10 September) is highlighted for the year 2019 in **(b)**. The locations of **(a)**–**(c)** are shown in Fig. 7c.

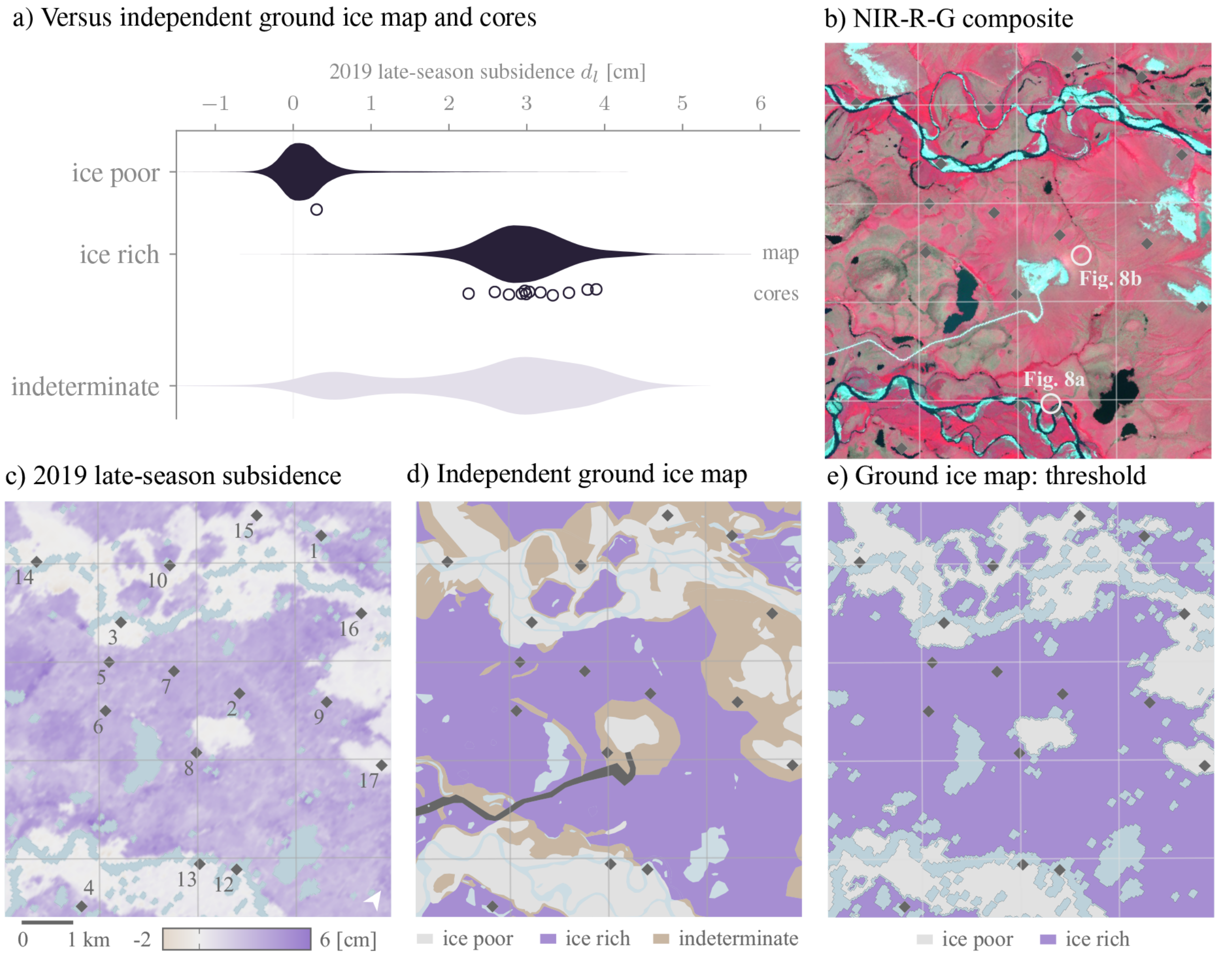

Figure 7. Assessment of late-season subsidence with respect to an independent ground ice map of the focus area defined in Fig. 5. **(a)** Kernel density distribution of d_l in 2019 over areas independently determined to be ice rich and ice poor. The markers just below the kernel density estimates show the observations at the boring locations (triangles in Fig. 5). **(b)** Sentinel-2 false-colour composite (Copernicus Sentinel, 2020) for the focus area defined in Fig. 2. **(c)** The estimated d_l, **(d)** the independently determined ground ice map, and **(e)** the ground ice classification obtained by thresholding d_l. The diamonds indicate points mentioned in Figs. 6 and 10.

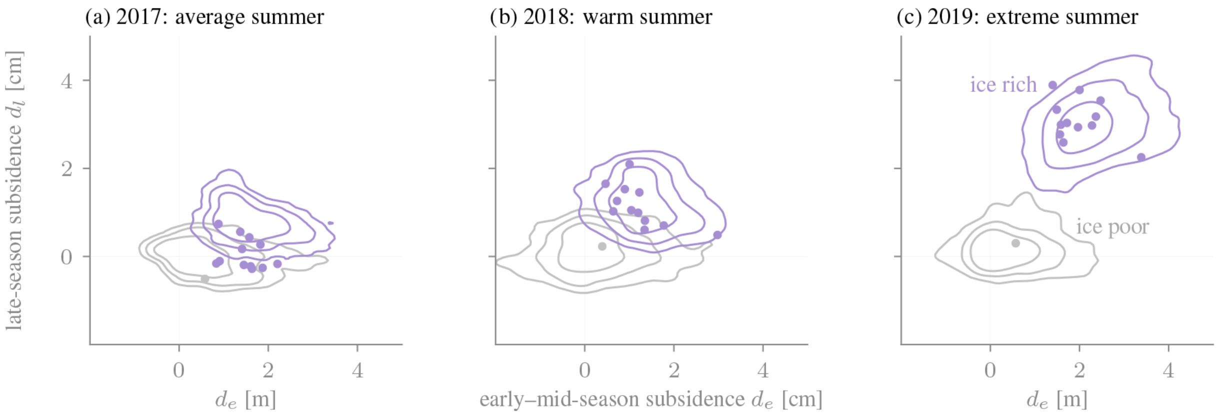

Figure 8. Contour plot of a kernel density estimate of the early–mid-season and late-season subsidence for ice rich (purple) and ice poor (grey), as determined independently by manual mapping (Fig. 7d). The markers correspond to the values observed at the location of the ice cores (triangles in Fig. 5). Negative values, corresponding to heave, are of comparable magnitude to the referencing accuracy of ~ 1 cm.

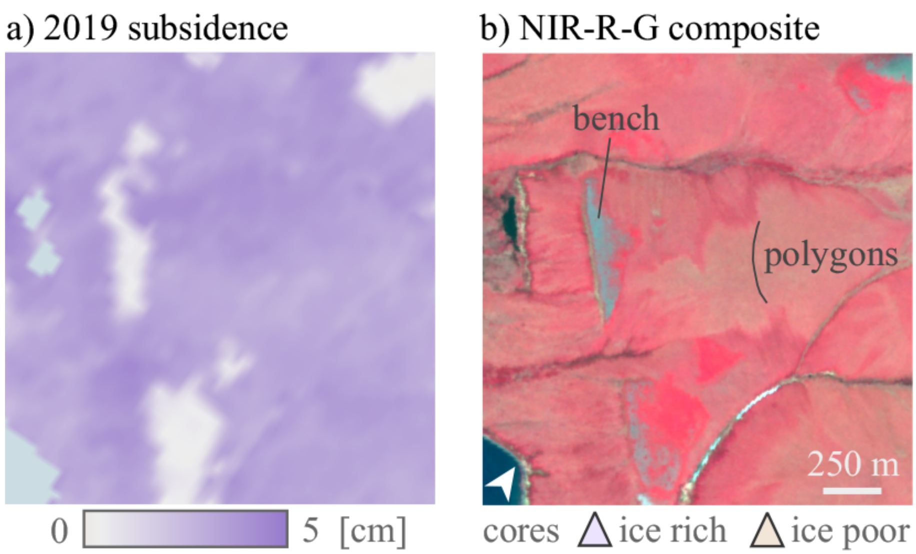

Figure 9. Late-season subsidence in 2019 **(a)** at the Tatchim Isua site (see Fig. 5 for its location) is smaller at the site of the gravelly bench, which appears grey in the false-colour composite (courtesy of Planet Labs, Inc.; Planet Team, 2020) in **(b)**, than the areas further upslope (right) and downslope (left). The triangles mark the location of the ice cores, with the colour indicating their ice content. Ice wedge polygons were observed in the field ~ 300 m upslope from the bench.

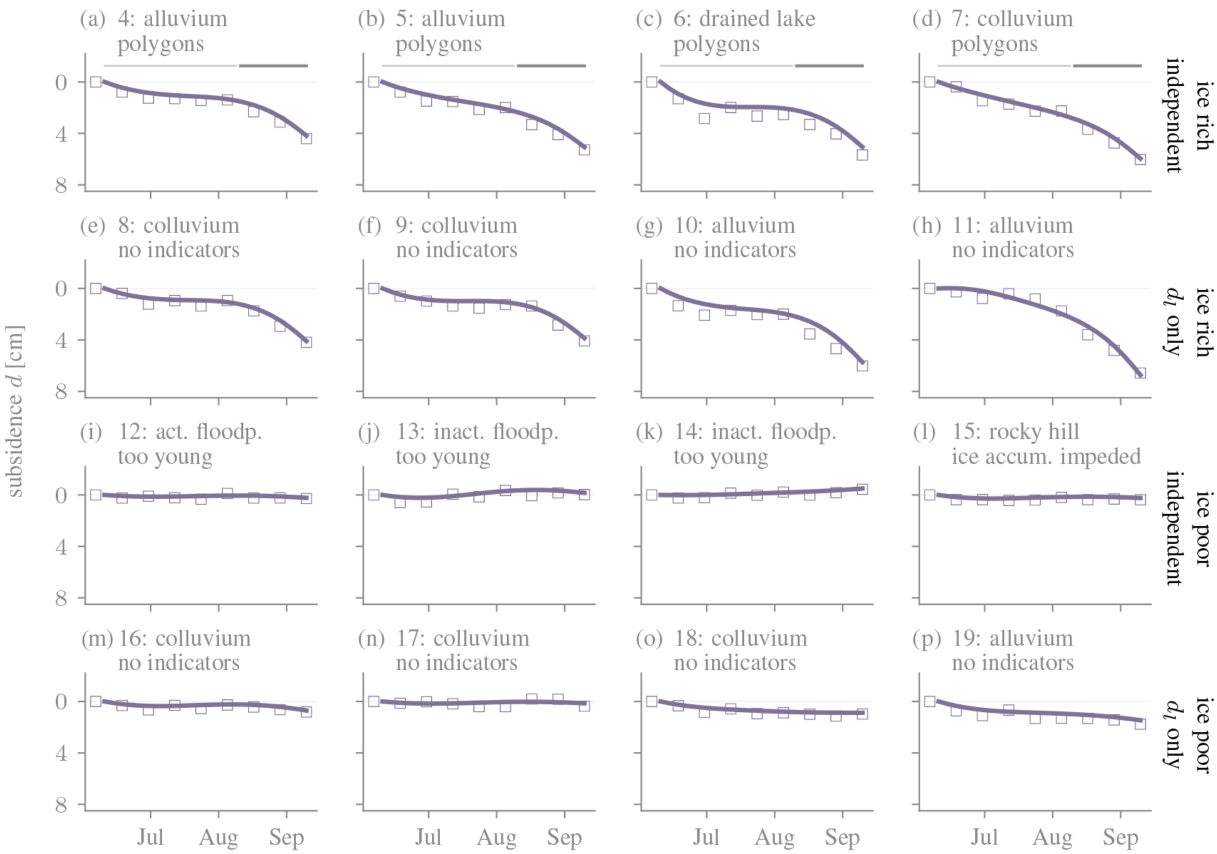

Figure 10. Subsidence time series (line: spline fit, markers: unconstrained) from 2019 for points shown in Figs. 7c and 5d). First row **(a–d)**: points that were independently determined to be ice rich; second row **(e–h)** indeterminate according to manual mapping, but $d_l > 2.5$ cm indicates they are ice rich; third row **(i–l)**: independently determined to be ice poor; fourth row **(m–p)**: indeterminate according to manual mapping, but d_l indicates they are ice poor.